

Article

Selective Catalytic Reduction of NO by NH₃ Using a Combination of Non-Thermal Plasma and Mn-Cu/ZSM5 Catalyst

Tao Zhu ^{1,2,*}, Xing Zhang ¹, Wenfeng Niu ¹, Yatao Liu ¹, Bo Yuan ¹, Zhenguo Li ² and Haibing Liu ³

¹ Institute of Atmospheric Environmental Management and Pollution Control, China University of Mining & Technology (Beijing), Beijing 100083, China; zhangxing@student.cumtb.edu.cn (X.Z.); n13393860390@163.com (W.N.); yataoliu@student.cumtb.edu.cn (Y.L.); yb20201215@163.com (B.Y.)

² National Engineering Laboratory for Mobile Source Emission Control Technology, China Automotive Technology & Research Center Co., Ltd., Tianjin 300300, China; lizhenguo@catarc.ac.cn

³ Solid Waste and Chemicals Management Technology Center, China Ministry of Ecology and Environment, Beijing 100029, China; liuhaibing@meescc.cn

* Correspondence: bamboozt@cumtb.edu.cn; Tel.: +86-10-62339170; Fax: +86-10-62339170

Received: 23 June 2020; Accepted: 20 August 2020; Published: 11 September 2020



Abstract: Dielectric barrier discharge (DBD) could generate non-thermal plasma (NTP) with the advantage of fast reactivity and high energy under atmosphere pressure and low-temperature. The presented work investigated the selective catalytic reduction (SCR) of nitric oxide (NO) using a combination of NTP and an Mn-Cu/ZSM5 catalyst with ammonia (NH₃) as a reductant. The experimental results illustrate that the plasma-assisted SCR process enhances the low-temperature catalytic performance of the Mn-Cu/ZSM5 catalyst significantly, and it exhibits an obvious improvement in the NO removal efficiency. The reaction temperature is maintained at 200 °C in order to simulate the exhaust temperature of diesel engine, and the 10% Mn-8% Cu/ZSM5 catalyst shows the highest NO removal performance with about 93.89% at an energy density of 500 J L⁻¹ and the selectivity to N₂ is almost 99%. The voltage, frequency and energy density have a positive correlation to NO removal efficiency, which is positively correlated with the power of NTP system. In contrast, the O₂ concentration has a negative correlation to the NO removal, and the NO removal efficiency cannot be improved when the NO removal process reaches reaction equilibrium in the NTP system.

Keywords: non-thermal plasma; Mn-Cu/ZSM5 catalyst; selective catalytic reduction; influence parameter; NO removal efficiency

1. Introduction

The environmental hazards of nitric oxides (NO_x) have been proved to be related to the photochemical smog and greenhouse effects closely in the last several decades. The wanton emission of NO_x poses great threats to the ecosystems, which not only causes a series of environmental problems, but also endangers human health [1–4]. The mobile sources emission is the main source of NO_x, especially the high-power diesel engines, and nitric oxide (NO) constitutes a great majority of NO_x. The selective catalytic reduction (SCR) of NO_x with ammonia (NH₃) is regarded as one of the most effective strategies for NO_x emission control owing to its reliable stability, which has been widely used in diesel engine [5–8]. However, the NH₃-SCR has a high operating temperature window (>350 °C), and the exhaust temperature of the diesel engine is usually 200 °C. The increasingly stringent emission regulations demand the development of high-performance NH₃-SCR available for low-temperature conditions [9,10].

The SCR catalyst is the core of NH_3 -SCR technology, and the V_2O_5 - WO_3 / TiO_2 catalyst shows excellent reactive activity, which possess desirable tolerance of SO_2 and high catalytic performance from 300 to 400 °C. However, a number of obstacles haunt this technology, such as a narrow work temperature window and poor N_2 selectivity [11–13]. Therefore, it is necessary to develop a low-temperature SCR catalyst with the wide temperature window. Manganese (Mn)-based SCR catalysts have been widely investigated for several years due to its high catalytic activity and superior low-temperature performance. In addition, it is generally believed that copper (Cu) has excellent catalytic performance as a promoter at low temperature, and it could strengthen the overall mechanical properties of the catalyst [14–20]. Wang et al. synthesized a lot of Mn-Cu/ZSM5 catalysts using the wetness impregnation method, and the result indicated that the incorporation of Mn improved the low-temperature activity of the SCR catalyst effectively [21]. Yan et al. designed a series of novel low-temperature $\text{Cu}_w\text{Mn}_y\text{Ti}_{1-y}\text{O}_x$ catalysts, in which CuO and MnO_x were as the active components and TiO_2 was as the support. The results suggested that the amount of acid sites increased significantly after adding Cu, and the NO_x removal efficiency of the $\text{Cu}_1\text{Mn}_{0.5}\text{Ti}_{0.5}\text{O}_x$ catalyst reached 90% at 200 °C [22]. The ZSM5 has been widely used as the support material of catalysts on account of its unique crystal structure, thermal stability, and excellent catalytic activity, and it has been reported that the framework of ZSM5 plays an important role in the selective catalytic reduction of NO [23,24].

Recently, the non-thermal plasma (NTP) technology has been proposed as a promising and effective in the treatment of gaseous pollutants [25–28]. The dielectric barrier discharges (DBD) appear well adapted to remove NO_x with high purification efficiency and low energy cost compared with other non-thermal gas discharges [29]. It is reported that there are two methods for NTP to remove NO. One method is to form higher valence oxides by oxidation, such as NO_2 , N_2O_5 , etc. The other method is to form N_2 and O_2 by reduction [30–32]. Wang et al. prepared a lot of bimetal oxide catalysts (M-Cu, M = Mn, Ce, Cr, Co, and Fe), and then he combined catalysts with NTP to evaluate the NO_x removal at various temperatures. The result showed that the bimetal oxide catalysts combined with NTP exhibited excellent NO_x removal efficiency [33]. Rajanikanth et al. used the barrier discharge corona assisted by V_2O_5 / TiO_2 catalyst to remove NO_x , and he found that the plasma-assisted catalytic process exhibited a remarkable improvement in NO removal efficiency [34].

NTP appears a wide foreground in the removal of NO_x from diesel engine due to its high conversion efficiency and easy installation, which could generate lots of free radicals like hydroxyl radical ($\cdot\text{OH}$), nitrogen radical ($\cdot\text{N}$), and oxygen radical ($\cdot\text{O}$). However, these active species are usually short-lived, which would disappear before entering the second catalyst stage. Therefore, the synergistic effect of a one-stage plasma-over-catalyst (POC) system is better than the two-stage plasma-followed-by-catalyst (PFC) hybrid system [35,36]. This research reports observations of an synergistic effect between NTP and Mn-Cu/ZSM5 catalysts in a one-stage POC reactor for NH_3 -selective-reduction of NO at 200 °C and investigates the influence parameters of NO removal in order to provide references for practical applications.

2. Results and Discussion

2.1. Characterizations of Mn-Cu/ZSM5 Catalysts

The characterizations of Mn-Cu/ZSM5 catalysts were carried out in this section, which could reveal the composition of catalysts concretely. In order to observe the micromorphology of the catalyst in detail, the 10% Mn-8% Cu/ZSM5 was selected as the representative to get SEM, HRTEM and EDS images, and the results are shown in Figure 1. It shows that the 10% Mn-8% Cu/ZSM5 catalyst is mainly constituted by pseudospherical particle. The HRTEM micrograph reveals that the lattice fringe of 10% Mn-8% Cu/ZSM5 catalyst was 2.5 Å, which could be assigned to the (111) crystal planes of crystalline CuO in accordance with the standard CuO card (JCPDS 01-1117). It illustrates that the target Cu was loaded on the surface of the 10% Mn-8% Cu/ZSM5 catalyst. Further, the EDS images of O, Al, Si, Mn and Cu elements were performed on the 10% Mn-8% Cu/ZSM5 catalyst, which indicates that

the active metal elements Mn and Cu were uniformly dispersed on the surface of the ZSM5 carrier. The Al and Si elements were derived from the ZSM5 carrier, and the O element was derived from the active metal oxides of the 10% Mn-8% Cu/ZSM5 catalyst in addition to the ZSM5 carrier.

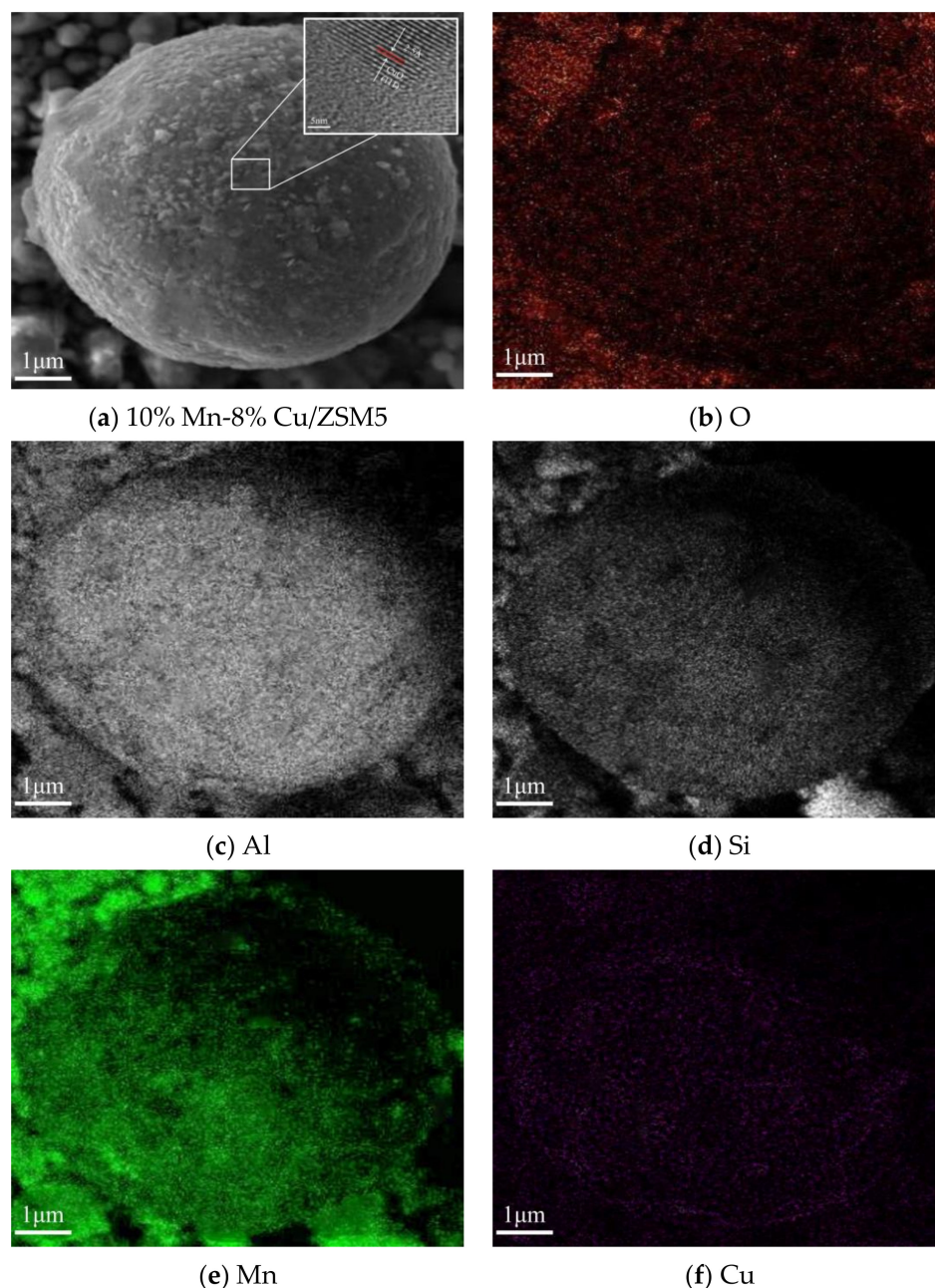


Figure 1. SEM, HRTEM and EDS images of the 10% Mn-8% Cu/ZSM5 catalyst.

The Brunauer–Emmett–Teller (BET) surface area, pore volume, and pore diameter of ZSM5 and Mn-Cu/ZSM5 catalysts are summarized in Table 1. Obviously, the BET surface area of the prepared catalysts decreased because the ZSM5 was impregnated with Mn and Cu metal elements, and the pore volume was reduced while the pore diameter increased. Li et al. investigated the relationship between the catalytic activity and specific surface areas, and he discovered that the larger specific surface area promoted the NO_x adsorption significantly because it could provide more acid sites for the catalytic reaction [37].

Table 1. Physical characteristics of ZSM5 and Mn-Cu/ZSM5 catalysts.

Sample	BET Surface Area (m ² /g)	Pore Volume (cm ³ /g)	Pore Diameter (nm)
ZSM5	388 ± 1.56	0.138 ± 0.01	1.46 ± 0.03
10% Mn-4% Cu/ZSM5	302 ± 1.62	0.107 ± 0.02	1.59 ± 0.01
10% Mn-6% Cu/ZSM5	296 ± 1.28	0.103 ± 0.01	1.62 ± 0.02
10% Mn-8% Cu/ZSM5	286 ± 2.28	0.101 ± 0.02	1.66 ± 0.01
10% Mn-10% Cu/ZSM5	283 ± 2.28	0.098 ± 0.01	1.70 ± 0.01

The XRD pattern of Mn-Cu/ZSM5 catalysts with different loadings of 4%, 6%, 8%, and 10% Cu are shown in Figure 2. The Mn was not found in the XRD pattern. On the one hand, a small amount of Mn-based metal oxide catalysts were present in the amorphous state. On the other hand, the Mnⁿ⁺ ions were incorporated into the Cu oxide lattice, and then it tends to form a solid solution during the calcinations based on related research [38,39]. Tang et al. found that the amorphous MnO_x played an important role in the removal of NO_x [40]. Boningari et al. revealed that amorphous MnO₂ was of higher activity if compared with crystalline MnO₂ for NO reduction [41]. Fang et al. reported that some Mn oxides are strongly associated with Cu oxides to form CuMn₂O₄, which was an active oxidation catalyst because of the easy electron transfer between Mn and Cu ions without a change in lattice, improving the lattice oxygen mobility and redox quality [42]. The (111) crystal planes of crystalline CuO were detected at 37°. Zhao et al. reported that the chemical forms of Cu species were present nearly exclusively in the form of oligomeric species and mononuclear ions [43].

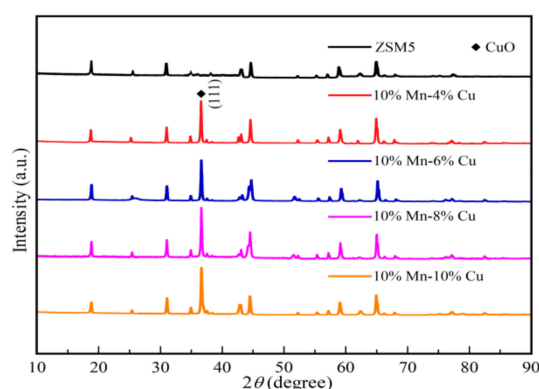
**Figure 2.** The XRD pattern of Mn-Cu/ZSM5 catalysts with different loadings of 4%, 6%, 8%, and 10% Cu, respectively.

Figure 3 shows the XPS pattern of Mn-Cu/ZSM5 catalysts with different loadings of 4%, 6%, 8%, and 10% Cu, respectively. As depicted in the picture, the Mn 2p_{3/2} spectra could be separated into three peaks, including Mn²⁺, Mn³⁺, and Mn⁴⁺. Table 2 displays the Mn valence binding energy distribution of Mn-Cu/ZSM5 catalysts, which indicates that Mn oxides are mainly in Mn³⁺ and Mn⁴⁺. The ion concentration of Mn³⁺ and Mn⁴⁺ reached maximum when the loading amount of Cu was 8%. Fang et al. revealed that every kind of pure MnO_x had its characteristic peak, and different MnO_x species played important roles in the SCR process. Furthermore, Mn₂O₃ and Mn₃O₄ species were active for an NO_x reduction based on the SCR performance [44]. Stanculescu et al. reported that the SCR catalysts containing Mn³⁺ appeared to be more active for NO_x reduction than those with Mn⁴⁺ [43]. According to the relevant research, the redox cycle between Mn and Cu with different chemical states and NO oxidation mechanism could be described by the following reactions [45–49].

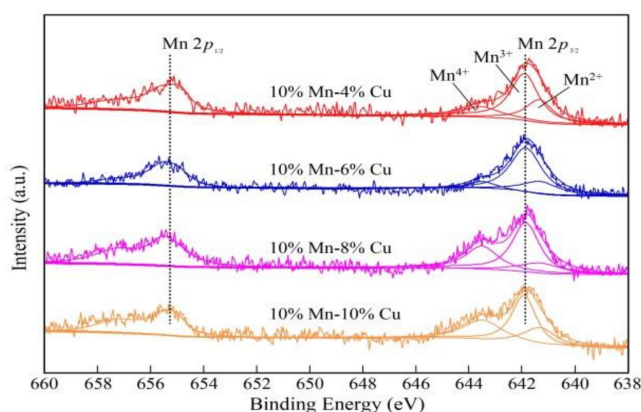


Figure 3. The XPS pattern of Mn-Cu/ZSM5 catalysts with different loadings of 4%, 6%, 8%, and 10% Cu, respectively.

Table 2. The Mn valence binding energy distribution of Mn-Cu/ZSM5 catalysts.

SCR Catalysts	Mn ²⁺ (eV)	Mn ³⁺ (eV)	Mn ⁴⁺ (eV)	N (Mn ³⁺ + Mn ⁴⁺)/n(Mn ^{x+})
10% MnO _x -4% Cu	641.2	642.0	643.6	0.82
10% MnO _x -6% Cu	641.2	642.0	643.5	0.85
10% MnO _x -8% Cu	641.1	641.9	643.4	0.87
10% MnO _x -10% Cu	641.2	641.9	643.5	0.86

2.2. Effect of Voltage on NO Removal Efficiency

Figure 4 displays that the voltage was positively correlated with the NO removal efficiency in range of 10–20 kV at a frequency of 1000 Hz. The tested concentration of NO and NH₃ were 300 ppm and 60 ppm, respectively. The NO removal efficiency was just 39.16% at a voltage of 20 kV only in the presence of NTP, and NO removal efficiency was 92.08% in combination of NTP and 10% Mn-8% Cu/ZSM5 catalyst, increased by 52.92%. The N₂ selectivity remained stable at nearly 99%. Du et al. found that more energy would be injected into the NTP system with the increase of voltage, and a lot of active species, free radicals, and high-energy electrons could generate under this condition [50]. On one hand, high-energy electrons could collide with H₂O and O₂ in the air. The ultimate result is that lots of active species and free radicals would generate in the NTP system, such as ·OH, ·O, and so on. On the other hand, high-energy electrons could collide with pollutant molecules directly or indirectly, and then break the chemical bonds. Clearly, the electric field strength was gradually increased with the voltage increasing. Therefore, the electric field intensity and quantity of plasma generated per unit time increased to the NO removal efficiency.

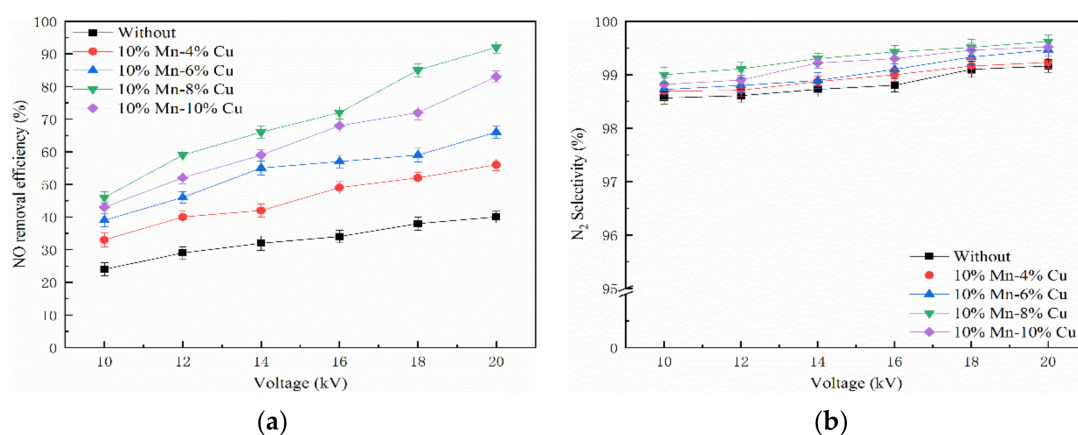


Figure 4. Effect of voltage on NO removal efficiency. (a) NO removal efficiency and (b) N₂ selectivity.

2.3. Effect of Frequency on NO Removal Efficiency

Figure 5 illustrates the effect of frequency on NO removal efficiency at a voltage of 20 kV. The tested concentration of NO and NH₃ were 300 ppm and 60 ppm, respectively. Obviously, the selectivity to N₂ was almost 99%, and the NO removal efficiency was proportional to the discharge frequency, which indicates that the NO removal efficiency was greatly affected by frequency. Zhu et al. found that the energy injected into the NTP system was positively correlated with frequency [51]. Compared with only plasma, the NO removal efficiency increased in the plasma–catalyst system. Among all the catalysts, the 10% Mn-8% Cu/ZSM5 catalyst shows the highest activity for NO removal. Meanwhile, it suggests that there was a significant synergistic effect between the NTP and Mn-Cu/ZSM5 catalyst. However, the NO removal efficiency tended to be gentle at high frequency, which indicates that the energy consumption of NO decreased compared to a low frequency. Yan et al. revealed that the gaseous benzene removal efficiency would increase with the increase of frequency because the energy imported to the reactor in unit time increased [52].

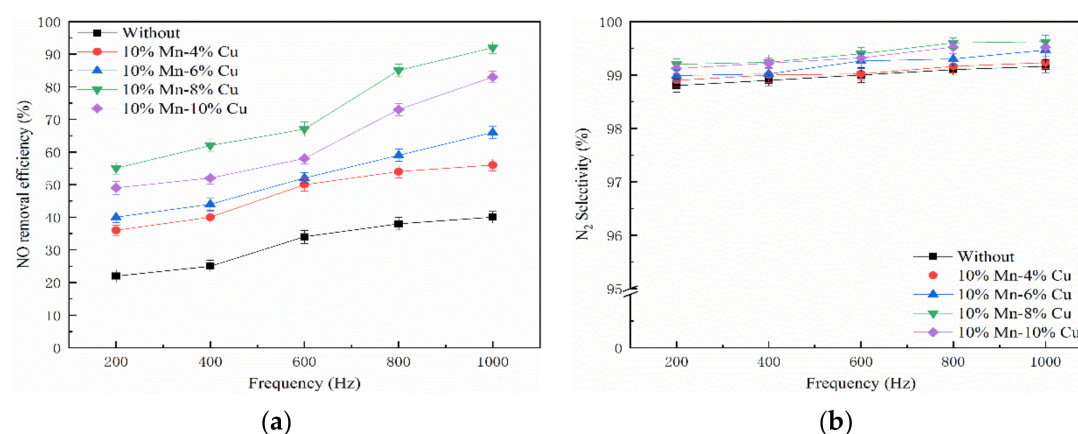


Figure 5. Effect of frequency on NO removal efficiency. (a) NO removal efficiency and (b) N₂ selectivity.

2.4. Effect of Energy Density on NO Removal

The discharge power is measured according to the V-Q Lissajous figure method [53], which is shown in Figure 6.

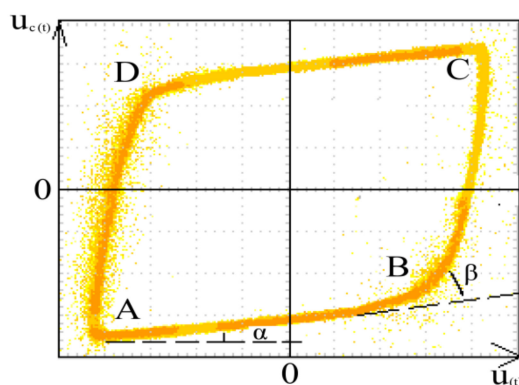


Figure 6. V-Q Lissajous graph.

The discharge power was given by Equation (5), and the energy density was calculated using Equation (6).

$$P = \frac{1}{T} \int_0^T u(t)i(t)dt = \frac{C_m}{T} \int_0^T \frac{du_c(t)}{dt} dt = fC_m \cdot S \quad (5)$$

$$\varepsilon = \frac{P}{Q} \quad (6)$$

In the equation, T is the period of discharge cycle, in s; $u(t)$ represents the high voltage applied between electrodes, in kV; $i(t)$ is the current changes with time, in A; f represents power frequency, in Hz; $u_c(t)$ is the voltage at both ends of C_m , in kV; C_m represents the measuring capacitance, which is 0.12 μF ; S is the area of Lissajous graphics. ε is the energy density, in J L^{-1} ; and Q is the gas flow, in L min^{-1} .

Figure 7 shows the variation of energy density and the NO removal efficiency. The tested concentration of NO and NH_3 was 300 ppm and 60 ppm, respectively. The NO removal efficiency was climbing up with the increase of energy density, and Mn-Cu/ZSM5 catalysts enhanced the NO removal efficiencies in the presence of NTP, which presents a straight line that approximated the proportional increase. The NO removal efficiency was only 41.66% without the catalyst at an energy density of 500 J L^{-1} , and NO removal efficiency was 93.89% in combination of NTP and 10% Mn-8% Cu/ZSM5 catalyst, increased by 52.23%, and the selectivity to N_2 is almost 99%. The results indicate that the 10% Mn-8% Cu catalyst with plasma exhibits the highest catalytic activity.

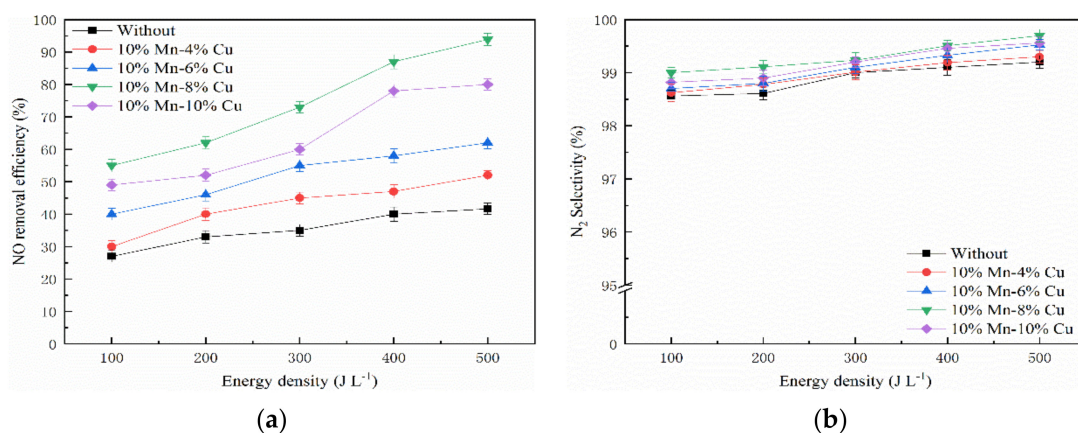


Figure 7. Effect of energy density on NO removal efficiency. (a) NO removal efficiency and (b) N_2 selectivity.

2.5. Effect of O₂ Concentration on NO Removal

The relationship between energy density and NO removal efficiency under different O₂ concentrations (0, 2%, 4%, 6%, and 8%) is shown as Figure 8, which is in combination with NTP and the 10% Mn-8% Cu/ZSM5 catalyst. The tested concentration of NO and NH₃ was 300 ppm and 60 ppm, respectively. The energy density varied from 100 to 500 J L⁻¹. The result indicates that the NO removal efficiency increased gradually with the energy density increasing, and then decreased with the increase of O₂ concentration under the same energy density. The N₂ selectivity shows a similar trend. This result is consistent with Zhao's results, and Zhao et al. revealed that the NO_x removal efficiency decreased with the O₂ concentration increasing, and he found that there was a critical O₂ concentration to make the NO_x removal efficiency zero [54]. According to relevant research, large quantities of active species would be generated when the O₂ concentration increased in the NTP system, such as ozone (O₃) and so on. Then, lots of NH₃ would be oxidized to NO molecules, which play a negative role in the removal of NO. As a final result, the NO and NH₃ were partially oxidized to NO₂ [55,56]. Therefore, the NO removal process is suppressed and the NO removal efficiency decreased. In the presence of O₂ and O₃, the following reactions would occur in the NTP system based on the relevant research [57–59].

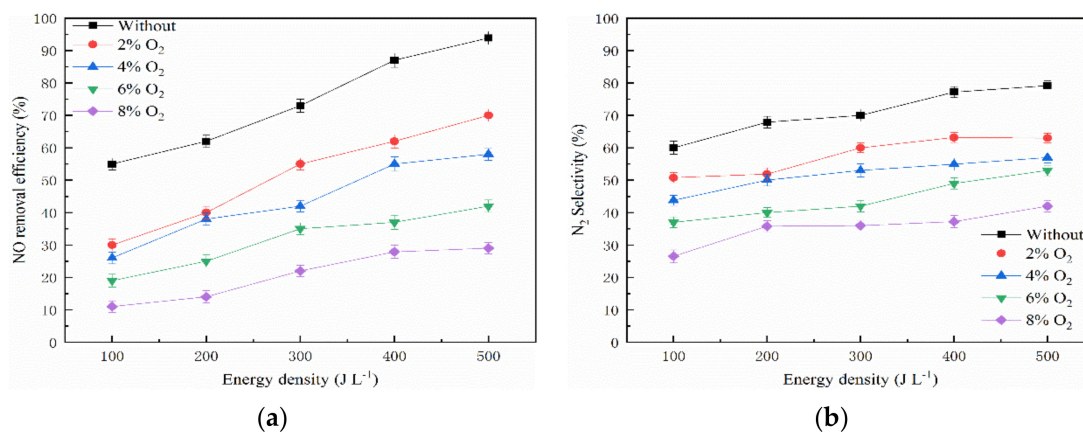
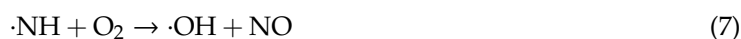


Figure 8. Effect of O₂ concentration on NO removal efficiency. (a) NO removal efficiency and (b) N₂ selectivity.

The relationship between energy density and NO₂ concentration is presented in Figure 9. In the presence of O₂ molecules, the NO₂ concentration increased slightly when the energy density was over 100 J L⁻¹, and then the NO₂ concentration remained stable with the energy density continually increasing. Ruggeri et al. revealed that NO₂ was a key reaction product in the catalytic reaction and the SCR reaction dominated the NO reduction with a catalyst below 200 °C [60]. The electric field of the reaction system was strengthened with the increase of energy density, and more NH₃ molecules participated in the reactions with O₂ and ·O, which led to new NO₂ molecule production. On the one hand, the active species O₃, ·O, and ·N formed in the plasma-catalyst system reacted with NO to form different NO_x. On the other hand, O₃ and ·O could react with NO to oxidize NO to NO₂. Koebel et al.

found that the NO would be oxidized to higher valence oxides because O₃ was more oxidative than O₂. So, the NO₂ was the main product in the presence of O₂ [61]. The oxidation of NO to NO₂ could be summarized as the following reactions [62–65].

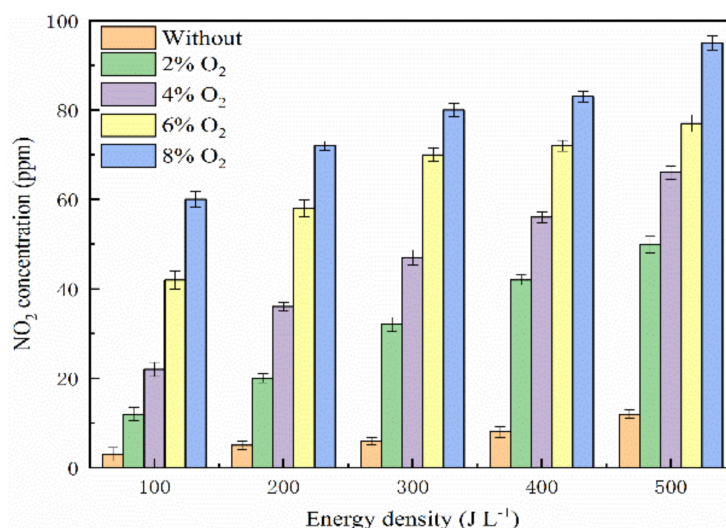
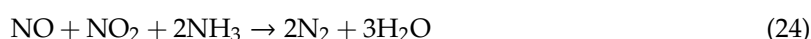
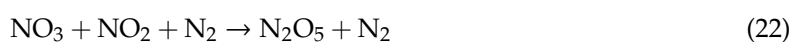


Figure 9. Effect of O₂ concentration on NO₂ concentration.

2.6. Effect of NH₃ Concentration on NO Removal

The effect of NH₃ concentration and energy density on NO removal efficiency is presented in Figure 10. The tested NO concentration was 300 ppm and the NH₃ concentration varied from 20 ppm to 100 ppm. The result indicates that the NO removal efficiency was affected by the addition of NH₃ significantly.

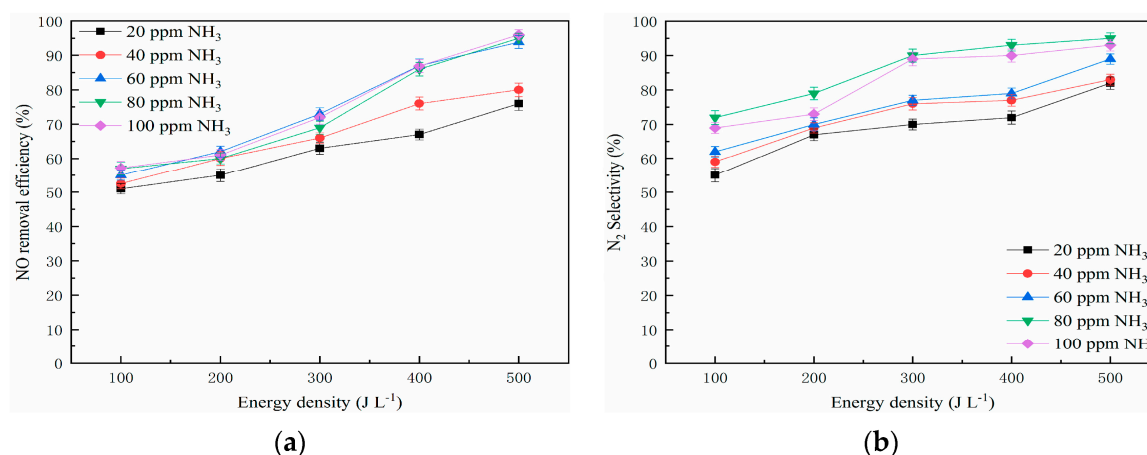


Figure 10. Effect of NH₃ concentration on NO removal efficiency. (a) NO removal efficiency and (b) N₂ selectivity.

In the presence of NH₃, there was higher probability of collision between NO molecules and high-energy electrons in the NTP system. As a result, the numbers of active species and free radicals were improved with the increase of energy density. When the NH₃ concentration increased in the NTP system, it is generally believed that the ammonia radical ($\cdot\text{NH}_2$) plays an important role in the NO_x removal. Wang et al. reported that the collision reactions of NO molecules were enhanced with the increase of NH₃ concentration, and this is because an enormous amount of free radicals would generate in the NTP system, such as NH₂ \cdot , NH \cdot , and H \cdot [66]. As a result, more NO molecules are removed under the same energy density. Therefore, the energy consumption decreased in the presence of NH₃ in the NTP system. However, the NO removal efficiency tends to stabilize at high NH₃ concentrations, which indicates that there is an optimal NH₃ concentration in combination of NTP and the Mn-Cu/ZSM5 catalyst. On the whole, the NO removal efficiency cannot be improved when the NO removal process reaches reaction equilibrium in the NTP system, even if the NH₃ concentration increased continuously. The main chemical reactions could be concluded as follows [67,68].



2.7. The Catalytic Long-Term Stability of the 10% Mn-8% Cu/ZSM5 Catalyst

The long-time stability is an important index to evaluate the NO removal efficiency of the 10% Mn-8% Cu/ZSM5 catalyst in the NTP system, which could provide basic research data for the practical applications. The tested concentration of NO and NH₃ was 300 ppm and 60 ppm, respectively. The reaction temperature was maintained at 200 °C, and the O₂ concentration was 0 and the energy density of plasma was 500 J L⁻¹. As can be seen from Figure 11, a 25 h continuous test was performed in this section, and the long-term stability of the 10% Mn-8% Cu/ZSM5 catalyst at an energy density of 500 J L⁻¹ was explored. The NO removal efficiency of the 10% Mn-8% Cu/ZSM5 catalyst was rather stable with a slight fluctuation around $\pm 1\%$ after the 25 h of continuous testing, and the NO removal efficiency remained at nearly 93%. At the same time, the N₂ selectivity remained stable at nearly 99%, which illustrates that there was almost no deactivation that occurred during the 25 h test at an energy density of 500 J L⁻¹, and further demonstrates that the 10% Mn-8% Cu/ZSM5 catalyst had excellent long-term stability in the NTP system.

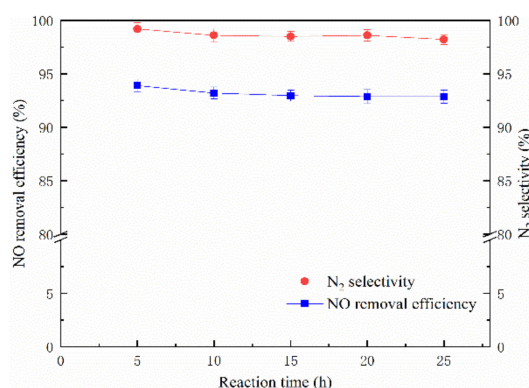


Figure 11. The catalytic long-term stability of the 10% Mn-8% Cu/ZSM5 catalyst.

3. Materials and Methods

3.1. Catalyst Preparation

ZSM5 (Si/Al = 25) was purchased from Nankai Catal. Corp. The Mn-Cu/ZSM5 catalysts were synthesized using the incipient wetness impregnation method. The $\text{Mn}(\text{NO}_3)_2$ and $\text{Cu}(\text{NO}_3)_2$ were dissolved in deionized water, and the corresponding proportion ZSM5 was added in solution. The active component Mn loading was 10 wt % and the target Cu loadings were 4 wt %, 6 wt %, 8 wt %, and 10 wt %, respectively. The ZSM5 and mixture of metal nitrates was heated for 2 h in the ohmic heating equipment, and then stirred for 5 h continuously. The obtained solid samples were dried at 100 °C, and then calcined for 5 h at 500 °C in air. Immediately, these catalysts were cooled down to room temperature under N_2 atmosphere. Finally, the Mn-Cu/ZSM5 catalysts were pressed, crushed, and sieved to 40–60 mesh to obtain suitable particles for the following experiments, which were noted as 10% Mn-4% Cu/ZSM5, 10% Mn-6% Cu/ZSM5, 10% Mn-8% Cu/ZSM5, and 10% Mn-10% Cu/ZSM5, respectively.

3.2. Catalyst Characterization

The structural and morphological properties of synthesized solid catalyst samples were characterized using scanning electron microscopy (SEM), high-resolution transmission electron microscopy (HRTEM), energy dispersive spectroscopy (EDS), X-ray diffraction (XRD), and X-ray photoelectron spectroscopy (XPS), respectively. The S80 JEOL (SEM, S80 JEOL, Tokyo Japan) was used to examine the microscopy of Mn-Cu/ZSM5 catalysts surface, and the HRTEM images were recorded on a Tecnai G2 F20 S-TWIN microscope (FEI, Hillsboro, OR, USA) at an accelerating voltage of 200 kV. The specific surface area and pore size of Mn-Cu/ZSM5 catalysts were calculated by the Brunauer–Emmett–Teller (BET) method and the Barrett–Joyner–Halenda (BJH) method. Prior to the measurements, these catalysts were outgassed overnight under vacuum. The EDS for the O, Al, Si, Mn, and Cu elements of Mn-Cu/ZSM5 catalysts were measured using an electric refrigeration X-ray energy spectrometer connected to SEM. The XRD measurement was carried out by an XRD-7000 S system (Shimadzu Corporation, Kyoto, Japan). The XPS was implemented on the surface analysis system (VG Multilab2000) with Al $K\alpha$ radiation ($h\nu = 1486.6$ eV) as the excitation source at 150 W, and the C1 s line at 284.6 eV was taken as the standard.

3.3. Experimental Setup

The schematic of the DBD plasma experiment is shown as Figure 12. The Mn-Cu/ZSM5 catalyst (2 mL, 40–60 mesh) was placed at the center of the DBD plasma reactor. The concentrations of Ar, O_2 , NO, and NH_3 in the experimental system were regulated by the mass flow controller (MFC), and then the gases flowed into the buffer tank. After they were mixed thoroughly, the gases were tested with the DBD plasma reactor, which could generate a NTP with the advantage of fast reactivity

and high energy at atmosphere pressure and low-temperature. The total gas flow was kept constant at 2 L min^{-1} , and the Ar was used as a carrier gas. The gas hourly space velocity (GHSV) was $60,000 \text{ h}^{-1}$. The temperature of the mixed gas was maintained at $200 \text{ }^\circ\text{C}$ in the NTP system. The plasma reactor was connected to an AC power, and the output waveform of DBD plasma was measured by Tektronix-TBS1102 digital oscilloscope, which was equipped with the current loop and P6015A high voltage probe. The concentrations of NO_x ($\text{NO} + \text{NO}_2$) and N_2O in the outlet gas were analyzed by an FT-IR gas analyzer (GASM ET DX 4000, Finland).

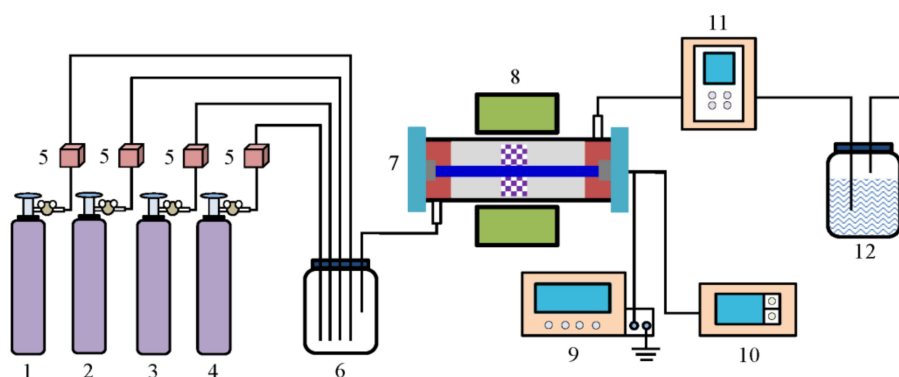


Figure 12. Schematic of the dielectric barrier discharge (DBD) plasma experiment. 1 Ar, 2 O_2 , 3 NO, 4 NH_3 , 5 Mass flow controller, 6 Buffer tank, 7 Plasma reactor, 8 Resistance furnace, 9 Power supply, 10 Digital oscilloscope, 11 Gas analyzer, and 12 Alkali absorption.

Figure 13 presents the DBD plasma reactor, which adopts the coaxial line structure. The dielectric tube was made of quartz and the sealing gaskets at both ends were made of polytetrafluoroethylene. The copper wire mesh was covered in the quartz, and it was used as a ground electrode. The diameter of dielectric tube was 20 mm, and the thickness of the dielectric tube was 2 mm. The length of the DBD plasma reactor was 500 mm.

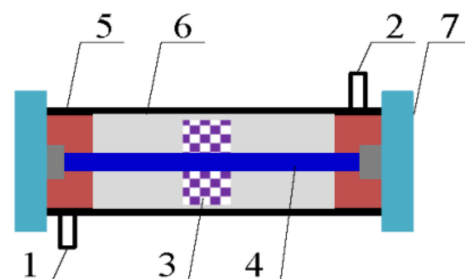


Figure 13. Schematic diagram of the plasma reactor structure. 1 Inlet, 2 Outlet, 3 Mn-Cu/ZSM5 catalyst, 4 Internal electrode, 5 Dielectric tube, 6 Ground electrode, and 7 Sealing gaskets.

The NO removal efficiency and N_2 selectivity were calculated by the following Equations (29) and (30). The analysis of experimental results was made in triplicate, and the error bar was used as an index to evaluate the difference between the average and measurement. The following Equations (31) and (32) were the average and error bar, respectively.

$$\text{NO removal efficiency (\%)} = \frac{\text{NO}_{\text{in}} - \text{NO}_{\text{xout}}}{\text{NO}_{\text{in}}} \times 100\% \quad (29)$$

$$\text{N}_2 \text{ selectivity (\%)} = \frac{\text{NO}_{\text{in}} - \text{NO}_{\text{xout}} - 2\text{N}_2\text{O}_{\text{out}}}{\text{NO}_{\text{in}} - \text{NO}_{\text{xout}}} \times 100\% \quad (30)$$

$$N_a = \frac{N_1 + N_2 + N_3}{3} \quad (31)$$

$$\text{Error bar} = \frac{\sum_{i=1}^3 |N_i - N_a|}{3} \quad (32)$$

where NO_{in} is the concentration of NO at the inlet of the DBD plasma reactor, $\text{N}_2\text{O}_{\text{out}}$ is the concentration of N_2O at the outlet of the DBD plasma reactor, and NO_{xout} is the concentration of NO_x ($\text{NO} + \text{NO}_2$) at the outlet of the DBD plasma reactor. N_a represents the average of three experimental results, N_1 , N_2 , and N_3 are the result of three experiments, respectively. N_i and N_a are the measured and averaged result, respectively.

4. Conclusions

The presented work proved that the plasma-assisted catalytic for NO removal was an effective method, which could provide a new strategy for the removal of NO_x from the diesel engine and it has huge potential for industrial applications in the future. The NO removal efficiency in the NTP system over Mn-Cu/ZSM5 catalysts was investigated, and the results indicate that the combination of NTP and Mn-Cu/ZSM5 catalyst promoted NO removal efficiency significantly. In addition, the influence parameters of voltage, frequency, energy density, and O_2 and NH_3 concentration on the NO removal efficiency were explored. The detailed experimental results are shown as follows:

- (1) The plasma-assisted SCR process exhibited an obvious improvement in NO removal efficiency, and 10% Mn-8% Cu/ZSM5 shows the highest catalytic activity with about 93.89% at an energy density of 500 J L^{-1} , and the selectivity to N_2 was almost 99%.
- (2) The voltage and frequency were positively correlated with the power of the NTP system. The NO removal efficiency increased with the voltage, frequency, and energy density increasing.
- (3) The O_2 concentration was negatively correlated with the NO removal in the NTP system. With the O_2 concentration increasing, the NO removal efficiency decreased significantly under the same energy density.
- (4) The NH_3 concentration was related to the NO removal closely, and the NO removal efficiency could not be improved when the NO removal process reached reaction equilibrium in the NTP system.

Author Contributions: All authors have contributed in various degrees to the analytical methods used, to the research concept, to the experiment design, to the acquisition of data, or analysis and interpretation of data, to draft the manuscript or to revise it critically for important intellectual content. All authors have read and agreed to the published version of the manuscript.

Funding: This work was supported by the National Engineering Laboratory for Mobile Source Emission Control Technology (NELMS2019A13), and the Major Science and Technology Projects of Shanxi Province (No. 20181102017), and the Shanxi Province Unveiled the List of Bidding Projects (No. 20191101007), and the Central Guide Local Science and Technology Development (No. 19943816G) and the Fundamental Research Funds for the Central Universities (No. 2009QH03).

Conflicts of Interest: The authors confirm that this article content has no conflict of interest.

References

1. Yang, Y.; Liu, J.; Liu, F.; Wang, Z.; Ding, J.; Huang, H. Reaction mechanism for NH_3 -SCR of NO_x over CuMn_2O_4 catalyst. *Chem. Eng. J.* **2019**, *361*, 578–587. [[CrossRef](#)]
2. Xu, L.; Yang, Q.; Hu, L.; Wang, D.; Peng, Y.; Shao, Z.; Lu, C.; Li, J. Insights over Titanium Modified FeMgO_x Catalysts for Selective Catalytic Reduction of NO_x with NH_3 : Influence of Precursors and Crystalline Structures. *Catalysts* **2019**, *9*, 560. [[CrossRef](#)]
3. An, D.H.; Zhang, X.Y.; Cheng, X.X.; Dong, Y. Performance of Mn-Fe-Ce/ GO_x for Catalytic Oxidation of Hg^0 and Selective Catalytic Reduction of NO_x in the Same Temperature Range. *Catalysts* **2018**, *8*, 399. [[CrossRef](#)]
4. Han, L.P.; Gao, M.; Hasegawa, J.; Li, S.X.; Shen, Y.J.; Li, H.R.; Shi, L.Y.; Zhang, D.S. SO_2 -Tolerant Selective Catalytic Reduction of NO_x over Meso- $\text{TiO}_2@ \text{Fe}_2\text{O}_3@ \text{Al}_2\text{O}_3$ Metal-Based Monolith Catalysts. *Environ. Sci. Technol.* **2019**, *53*, 6462–6473. [[CrossRef](#)] [[PubMed](#)]

5. Gao, F.Y.; Tang, X.L.; Yi, H.H.; Zhao, S.Z.; Li, C.L.; Li, J.Y.; Shi, Y.R.; Meng, X.M. A Review on Selective Catalytic Reduction of NO_x by NH₃ over Mn-Based Catalysts at Low Temperatures: Catalysts, Mechanisms, Kinetics and DFT Calculations. *Catalysts* **2017**, *7*, 199. [[CrossRef](#)]
6. Gholami, R.; Stere, C.E.; Goguet, A.; Hardacre, C. Non-thermal-plasma-activated de-NO_x catalysis. *Philos. Trans. R. Soc. A Math. Phys. Eng. Sci.* **2017**, *376*, 0054. [[CrossRef](#)] [[PubMed](#)]
7. Mohapatro, S.; Rajanikanth, B.S. Dielectric barrier discharge cascaded with red mud waste to enhance NO_x removal from diesel engine exhaust. *IEEE Trans. Dielectr. Electr. Insul.* **2012**, *19*, 641–647. [[CrossRef](#)]
8. Miessner, H.; Francke, K.P.; Rudolph, R.; Hammer, T. NO_x removal in excess oxygen by plasma-enhanced selective catalytic reduction. *Catal. Today* **2002**, *75*, 325–330. [[CrossRef](#)]
9. Zhou, X.; Yu, F.; Sun, R.B.; Tian, J.Q.; Wang, Q.; Dai, B.; Dan, J.M.; Pfeiffer, H. Two-dimensional MnFeCo layered double oxide as catalyst for enhanced selective catalytic reduction of NO_x with NH₃ at low temperature (25–150 °C). *Appl. Catal. A Gen.* **2020**, *592*, 117432. [[CrossRef](#)]
10. Damma, D.; Ettireddy, P.R.; Reddy, B.M.; Smirniotis, P.G. A Review of Low Temperature NH₃-SCR for Removal of NO_x. *Catalysts* **2019**, *9*, 349. [[CrossRef](#)]
11. Xin, Y.; Li, H.; Zhang, N.N.; Li, Q.; Zhang, Z.L.; Cao, X.M.; Hu, P.; Zheng, L.R.; Anderson, J.A. Molecular-Level Insight into Selective Catalytic Reduction of NO_x with NH₃ to N₂ over a Highly Efficient Bifunctional V- α -MnO_x Catalyst at Low Temperature. *ACS Catal.* **2018**, *8*, 4937–4949. [[CrossRef](#)]
12. Lopez-Hernandez, I.; Mengual, J.; Palomares, A.E. The Influence of the Support on the Activity of Mn-Fe Catalysts Used for the Selective Catalytic Reduction of NO_x with Ammonia. *Catalysts* **2020**, *10*, 63. [[CrossRef](#)]
13. Wang, R.H.; Hao, Z.F.; Li, Y.; Liu, G.Q.; Zhang, H.; Wang, H.T.; Xia, Y.G.; Zhan, S.H. Relationship between structure and performance of a novel highly dispersed MnO_x on Co-Al layered double oxide for low temperature NH₃-SCR. *Appl. Catal. B Environ.* **2019**, *258*, 117983. [[CrossRef](#)]
14. Li, L.C.; Wang, Y.S.; Zhang, L.; Yu, Y.X.; He, H.B. Low-Temperature Selective Catalytic Reduction of NO_x on MnO₂ Octahedral Molecular Sieves (OMS-2) Doped with Co. *Catalysts* **2020**, *10*, 396. [[CrossRef](#)]
15. Han, L.P.; Cai, S.X.; Gao, M.; Hasegawa, J.; Wang, P.L.; Zhang, J.P.; Shi, L.Y.; Zhang, D.S. Selective Catalytic Reduction of NO_x with NH₃ by Using Novel Catalysts: State of the Art and Future Prospects. *Chem. Rev.* **2019**, *119*, 10916–10976. [[CrossRef](#)]
16. You, Y.C.; Chen, S.Y.; Li, J.Y.; Zeng, J.; Chang, H.Z.; Ma, L.; Li, J.H. Low-temperature selective catalytic reduction of N₂O by CO over Fe-ZSM5 catalysts in the presence of O₂. *J. Hazard. Mater.* **2020**, *383*, 121117. [[CrossRef](#)]
17. Bozbag, S.E.; Sanli, D.; Ozener, B.; Hisar, G.; Erkey, C. An Aging Model of NH₃ Storage Sites for Predicting Kinetics of NH₃ Adsorption, Desorption and Oxidation over Hydrothermally Aged Cu-Chabazite. *Catalysts* **2020**, *10*, 411. [[CrossRef](#)]
18. Zhu, T.; Zhang, X.; Bian, W.J.; Han, Y.W.; Liu, T.S.; Liu, H.B. DeNO_x of Nano-Catalyst of Selective Catalytic Reduction Using Active Carbon Loading MnO_x-Cu at Low Temperature. *Catalysts* **2020**, *10*, 135. [[CrossRef](#)]
19. Husnain, N.; Wang, E.L.; Fareed, S. Low-Temperature Selective Catalytic Reduction of NO with NH₃ over Natural Iron Ore Catalyst. *Catalysts* **2019**, *9*, 956. [[CrossRef](#)]
20. Wang, C.; Wang, J.; Wang, J.Q.; Wang, Z.X.; Chen, Z.X.; Li, X.L.; Shen, M.Q.; Yan, W.J.; Kang, X. The Role of Impregnated Sodium Ions in Cu/SSZ-13 NH₃-SCR Catalysts. *Catalysts* **2018**, *8*, 593. [[CrossRef](#)]
21. Wang, T.; Zhang, X.Y.; Liu, J.; Liu, H.Z.; Wang, Y.; Sun, B.M. Effects of temperature on NO_x removal with Mn-Cu/ZSM5 catalysts assisted by plasma. *Appl. Therm. Eng.* **2018**, *130*, 1224–1232. [[CrossRef](#)]
22. Yan, Q.H.; Chen, S.N.; Zhang, C.; Wang, Q.; Louis, B. Synthesis and catalytic performance of Cu₁Mn_{0.5}Ti_{0.5}O_x mixed oxide as low-temperature NH₃-SCR catalyst with enhanced SO₂ resistance. *Appl. Catal. B Environ.* **2018**, *238*, 236–247. [[CrossRef](#)]
23. Wen, Z.C.; Du, M.M.; Li, Y.; Wang, Z.H.; Xu, J.R.; Cen, K.F. Quantum chemistry study on the oxidation of NO catalyzed by ZSM5 supported Mn/Co-Al/Ce. *J. Theor. Comput. Chem.* **2017**, *16*, 1750044. [[CrossRef](#)]
24. Jodlowski, P.J.; Kuteranski, L.; Jedrzejczyk, R.J.; Chlebda, D.; Gancarczyk, A.; Basag, S.; Chmielarz, L. DeNO_x Abatement Modelling over Sonically Prepared Copper USY and ZSM5 Structured Catalysts. *Catalysts* **2017**, *7*, 205. [[CrossRef](#)]
25. Zhu, T.; Wang, R.N.; Bian, W.J.; Chen, Y.; Jing, W.D. Advanced oxidation technology for H₂S odor gas using non-thermal plasma. *Plasma Sci. Technol.* **2018**, *20*, 054007. [[CrossRef](#)]
26. Pan, H.; Qiang, Y. Promotion of Non-thermal Plasma on Catalytic Reduction of NO_x by C₃H₈ Over Co/BEA Catalyst at Low Temperature. *Plasma Chem. Plasma P.* **2014**, *34*, 811–824. [[CrossRef](#)]

27. Nguyen, D.B.; Nguyen, V.T.; Heo, I.J.; Mok, Y.S. Removal of NO_x by selective catalytic reduction coupled with plasma under temperature fluctuation condition. *J. Ind. Eng. Chem.* **2019**, *72*, 400–407. [[CrossRef](#)]
28. Zhu, T.; Bian, W.J.; Ma, M.F.; Ye, W.L.; Wang, R.N.; Zhang, X. Influence of gas atmosphere on synergistic control of mercury and dioxin by non-thermal plasma. *Plasma Sci. Technol.* **2019**, *21*, 044006. [[CrossRef](#)]
29. Broer, S.; Hammer, T. Selective catalytic reduction of nitrogen oxides by combining a non-thermal plasma and a V₂O₅-WO₃/TiO₂ catalyst. *Appl. Catal. B Environ.* **2000**, *28*, 101–111. [[CrossRef](#)]
30. Guan, B.; Lin, H.; Cheng, Q.; Huang, Z. Removal of NO_x with Selective Catalytic Reduction Based on Nonthermal Plasma Preoxidation. *Ind. Eng. Chem. Res.* **2011**, *50*, 5401–5413. [[CrossRef](#)]
31. Chen, J.X.; Pan, K.L.; Yu, S.J.; Yen, S.Y.; Chang, M.B. Combined fast selective reduction using Mn-based catalysts and nonthermal plasma for NO_x removal. *Environ. Sci. Pollut. Res.* **2017**, *24*, 21496–21508. [[CrossRef](#)] [[PubMed](#)]
32. Wang, T.; Liu, H.Z.; Zhang, X.Y.; Guo, Y.H.; Zhang, Y.S.; Wang, Y.; Sun, B.M. A plasma-assisted catalytic system for NO removal over CuCe/ZSM-5 catalysts at ambient temperature. *Fuel Process. Technol.* **2017**, *158*, 199–205. [[CrossRef](#)]
33. Wang, T.; Liu, H.Z.; Yang, B.; Sun, B.M.; Xiao, H.P.; Zhang, Y.S. Effect of plasma-catalyst system on NO removal using M-Cu (M=Mn, Ce, Cr, Co, and Fe) catalysts. *Jpn. J. Appl. Phys.* **2016**, *55*, 116202. [[CrossRef](#)]
34. Rajanikanth, B.S.; Ravi, V. DeNO_x study in diesel engine exhaust using barrier discharge corona assisted by V₂O₅/TiO₂ catalyst. *Plasma Sci. Technol.* **2004**, *6*, 2411–2415. [[CrossRef](#)]
35. Sun, Q.; Zhu, A.M.; Yang, X.F.; Niu, J.H.; Xu, Y.; Song, Z.M.; Liu, J. Selective catalytic reduction of NO_x in dielectric barrier discharge plasmas. *Eur. Phys. J. Appl. Phys.* **2005**, *30*, 129–133. [[CrossRef](#)]
36. Kwak, J.H.; Peden, C.H.F.; Szanyi, J. Non-thermal plasma-assisted NO_x reduction over Na-Y zeolites: The promotional effect of acid sites. *Catal. Lett.* **2006**, *109*, 1–6. [[CrossRef](#)]
37. Li, L.; Wang, L.S.; Pan, S.W.; Wei, Z.L.; Huang, B.C. Effects of cerium on the selective catalytic reduction activity and structural properties of manganese oxides supported on multi-walled carbon nanotubes catalysts. *Chin. J. Catal.* **2013**, *34*, 1087–1097. [[CrossRef](#)]
38. Fan, X.Y.; Qiu, F.M.; Yang, H.S.; Tian, W.; Hou, T.F.; Zhang, X.B. Selective catalytic reduction of NO_x with ammonia over Mn-CeO_x/TiO₂-carbon nanotube composites. *Catal. Commun.* **2011**, *12*, 1298–1301. [[CrossRef](#)]
39. Jiang, L.J.; Liu, Q.C.; Zhao, Q.; Ren, S.; Kong, M.; Yao, L.; Meng, F. Promotional effect of Ce on the SCR of NO with NH₃ at low temperature over MnO_x supported by nitric acid-modified activated carbon. *Res. Chem. Intermed.* **2018**, *44*, 1729–1744. [[CrossRef](#)]
40. Tang, X.L.; Hao, J.M.; Xu, W.G.; Li, J.H. Low temperature selective catalytic reduction of NO_x with NH₃ over amorphous MnO_x catalysts prepared by three methods. *Catal. Commun.* **2006**, *8*, 329–334. [[CrossRef](#)]
41. Boningari, T.; Ettireddy, P.R.; Somogyvari, A.; Liu, Y.; Vorontsov, A.; McDonald, C.A.; Smirniotis, P.G. Influence of elevated surface texture hydrated titania on Ce-doped Mn/TiO₂ catalysts for the low-temperature SCR of NO_x under oxygen-rich conditions. *J. Catal.* **2015**, *325*, 145–155. [[CrossRef](#)]
42. Fang, D.; Xie, J.L.; Mei, D.; Zhang, Y.M.; He, F.; Liu, X.Q.; Li, Y.M. Effect of CuMn₂O₄ spinel in Cu-Mn oxide catalysts on selective catalytic reduction of NO_x with NH₃ at low temperature. *RSC Adv.* **2014**, *4*, 25540. [[CrossRef](#)]
43. Zhao, Z.W.; Li, E.W.; Qin, Y.; Liu, X.L.; Zou, Y.; Wu, H.; Zhu, T.Y. Density functional theory (DFT) studies of vanadium-titanium based selective catalytic reduction (SCR) catalysts. *J. Environ. Sci. China* **2020**, *90*, 119–137. [[CrossRef](#)] [[PubMed](#)]
44. Fang, D.; Xie, J.L.; Hu, H.; Yang, H.; He, F.; Fu, Z.B. Identification of MnO_x species and Mn valence states in MnO_x/TiO₂ catalysts for low temperature SCR. *Chem. Eng. J.* **2015**, *271*, 23–30. [[CrossRef](#)]
45. Stanciulescu, M.; Caravaggio, G.; Dobri, A.; Moir, J.; Burich, R.; Charland, J.P.; Bulsink, P. Low-temperature selective catalytic reduction of NO_x with NH₃ over Mn-containing catalysts. *Appl. Catal. B Environ.* **2012**, *123*, 229–240. [[CrossRef](#)]
46. Jiang, B.Q.; Liu, Y.; Wu, Z.B. Low-temperature selective catalytic reduction of NO on MnO_x/TiO₂ prepared by different methods. *J. Hazard. Mater.* **2009**, *162*, 1249–1254. [[CrossRef](#)]
47. Brookshear, D.W.; Nam, J.G.; Nguyen, K.; Toops, T.J.; Binder, A. Impact of sulfation and desulfation on NO_x reduction using Cu-chabazite SCR catalysts. *Catal. Today* **2015**, *258*, 359–366. [[CrossRef](#)]
48. Samojeden, B.; Grzybek, T. The influence of the promotion of N-modified activated carbon with iron on NO removal by NH₃-SCR (Selective catalytic reduction). *Energy* **2016**, *116*, 1484–1491. [[CrossRef](#)]

49. Salazar, M.; Hoffmann, S.; Singer, V.; Becker, R.; Grunert, W. Hybrid catalysts for the selective catalytic reduction (SCR) of NO by NH₃ center dot On the role of fast SCR in the reaction network. *Appl. Catal. B Environ.* **2016**, *199*, 433–438. [[CrossRef](#)]
50. Du, C.M.; Wang, J.; Zhang, L.; Li, H.X.; Liu, H.; Xiong, Y. The application of a non-thermal plasma generated by gas-liquid gliding arc discharge in sterilization. *New J. Phys.* **2012**, *14*, 013010. [[CrossRef](#)]
51. Zhu, T.; Zhang, X.; Ma, M.F.; Wang, L.F.; Xue, Z.Y.; Hou, Y.M.; Ye, Z.F.; Liu, T.S. 1,2,4-trichlorobenzene decomposition using non-thermal plasma technology. *Plasma Sci. Technol.* **2020**, *22*, 034011. [[CrossRef](#)]
52. Yan, X.F.; Hu, Z. Experiment and analysis on the treatment of gaseous benzene using pulsed corona discharge plasma. *Plasma Sci. Technol.* **2004**, *6*, 2241–2246.
53. Liang, W.J.; Ma, L.; Li, J.; Li, J.X.; Zheng, F. Control of Hydrogen Sulfide by a Wire-Tube Dielectric Barrier Discharge AC Plasma Reactor. *CLEAN-Soil Air Water* **2012**, *40*, 586–591. [[CrossRef](#)]
54. Zhao, G.B.; Garikipati, S.V.B.; Hu, X.D.; Argyle, M.D.; Radosz, M. Effect of oxygen on nonthermal plasma reactions of nitrogen oxides in nitrogen. *AIChE J.* **2005**, *51*, 1800–1812. [[CrossRef](#)]
55. Liu, Y.H.C.; Zhang, R.X.; Hou, H.Q.; Chen, S.P.; Zhang, R.N. NO reduction using low-temperature SCR assisted by a DBD method. *Plasma Sci. Technol.* **2018**, *20*, 014002. [[CrossRef](#)]
56. Kuwahara, T.; Yoshida, K.; Kuroki, T.; Hanamoto, K.; Sato, K.; Okubo, M. High Reduction Efficiencies of Adsorbed NO_x in Pilot-Scale Aftertreatment Using Nonthermal Plasma in Marine Diesel-Engine Exhaust Gas. *Energies* **2019**, *12*, 3800. [[CrossRef](#)]
57. Babaie, M.; Kishi, T.; Arai, M.; Zama, Y.; Furuhashi, T.; Ristovski, Z.; Rahimzadeh, H.; Brown, R. Influence of non-thermal plasma after-treatment technology on diesel engine particulate matter composition and NO_x concentration. *Int. J. Environ. Sci. Technol.* **2015**, *13*, 221–230. [[CrossRef](#)]
58. Hammer, T.; Kappes, T.; Baldauf, M. Plasma catalytic hybrid processes: Gas discharge initiation and plasma activation of catalytic processes. *Catal. Today* **2004**, *89*, 5–14. [[CrossRef](#)]
59. Li, J.H.; Ke, R.; Li, W.; Hao, J.M. Mechanism of selective catalytic reduction of NO over Ag/Al₂O₃ with the aid of non-thermal plasma. *Catal. Today* **2008**, *139*, 49–58. [[CrossRef](#)]
60. Ruggeri, M.P.; Nova, I.; Tronconi, E.; Pihl, J.A.; Toops, T.J.; Partridge, W.P. In-situ DRIFTS measurements for the mechanistic study of NO oxidation over a commercial Cu-CHA catalyst. *Appl. Catal. B Environ.* **2015**, *166*, 181–192. [[CrossRef](#)]
61. Koebel, M.; Madaia, G.; Elsener, M. Selective catalytic reduction of NO and NO₂ at low temperatures. *Catal. Today* **2002**, *73*, 239–247. [[CrossRef](#)]
62. Guo, X.R.; Ha, K.H.; Du, D.F. New Experiment of Diesel Exhaust Treatment by Atmospheric Pressure Plasma-Wood Fiber Combination. *Catalysts* **2020**, *10*, 577. [[CrossRef](#)]
63. Miessner, H.; Francke, K.P.; Rudolph, R. Plasma-enhanced HC-SCR of NO_x in the presence of excess oxygen. *Appl. Catal. B Environ.* **2002**, *36*, 53–62. [[CrossRef](#)]
64. McAdams, R.; Beech, P.; Shawcross, J.T. Low Temperature Plasma Assisted Catalytic Reduction of NO_x in Simulated Marine Diesel Exhaust. *Plasma Chem. Plasma P.* **2008**, *28*, 159–171. [[CrossRef](#)]
65. Hammer, T. Non-thermal plasma application to the abatement of noxious emissions in automotive exhaust gases. *Plasma Sources Sci. T.* **2002**, *11*, A196. [[CrossRef](#)]
66. Wang, Z.Y.; Kuang, H.L.; Zhang, J.F.; Chu, L.L.; Ji, Y.L. Nitrogen oxide removal by non-thermal plasma for marine diesel engines. *RSC Adv.* **2019**, *9*, 5402–5416. [[CrossRef](#)]
67. Park, S.Y.; Deshwal, B.R.; Moon, S.H. NO_x removal from the flue gas of oil-fired boiler using a multistage plasma-catalyst hybrid system. *Fuel Process. Technol.* **2008**, *89*, 540–548. [[CrossRef](#)]
68. Talebizadeh, P.; Babaie, M.; Brown, R.; Rahimzadeh, H.; Ristovski, Z.; Arai, M. The role of non-thermal plasma technique in NO_x treatment: A review. *Renew. Sustain. Energy Rev.* **2014**, *40*, 886–901. [[CrossRef](#)]

